SCIENTIFIC REPORTS
nature research

OPEN

Preparation of TiO_2-modified Biochar and its Characteristics of Photo-catalysis Degradation for Enrofloxacin

Wen Wang[1,4], Jing Zhang[1,4], Tianya Chen[1], Jing Sun[1], Xiulan Ma[1*], Yujun Wang[1], Jihong Wang[1] & Zhonglei Xie[2,3*]

In order to solve the problem that the traditional biochar(BC) has insufficient removal ability of enrofloxacin and TiO_2 is difficult to recycle. In this study, TiO_2-modified biochar composites were prepared by impregnation method. Through characterization analysis, The BET specific surface area results indicated that after loading TiO_2, the specific surface area of TiO_2-biochar(Ti-BC), TiO_2-ironized biochar(Ti-FBC) and TiO_2-alkaline biochar(Ti-KBC) increased by 4.34, 10.43 and 11.52 times, respectively. The analysis results of SEM, EDS, FT-IR, XRD and XPS showed that TiO_2 was supported on biochar in the anatase state. The UV-vis DRS measurement showed that the band width of Ti-KBC was the smallest and the best catalytic activity. Under 15 W UV lamp (254 nm) irradiation, the photocatalytic degradation process of enrofloxacin by different biochar accords with the first-order kinetic equation. Ti-KBC showed best degradation effect under different initial concentrations of enrofloxacin. When the pH of the solution was 5.0 and the dosage of Ti-KBC was at 2.5 $g \cdot L^{-1}$, the enrofloxacin degradation rate of 100 $mg \cdot L^{-1}$ reached 85.25%. The quenching test confirmed that the active substance $O_2\bullet^-$ played a major role in the photocatalytic degradation process. After five cycles of the test, the degradation rate of Ti-KBC for enrofloxacin was 77.14%, which was still better than that of BC, Ti-BC and Ti-FBC.

Enrofloxacin is the third-generation fluoroquinolone antibiotic which was synthesized in 1987 and is widely used in livestock and aquaculture as antibacterial drugs, because of its highly efficient against mycoplasma[1]. The excessive use of enrofloxacin has also been resulted in a series of pollution problems and there have been many reports on the excessive detection of enrofloxacin in the surface water near the farm[2]. The study found that after the enrofloxacin solution was administered to pigs, the amount of enrofloxacin in the excreta reached 34.44–78.42 $mg \cdot kg^{-1}$ [3] Enrofloxacin stays in the natural environment for a long time and produces "super bacteria", which poses a potential threat to human health[4]. Therefore, it is of great practical significance to explore ways to remove enrofloxacin remaining in the environment.

Biochar is a kind of solid matter which is formed by pyrolysis of biochar raw materials such as corn stover and wood chips under oxygen-limited conditions, and has strong adsorption capacity for pollutants[5]. Because of its rich surface functional groups and large specific surface area[6], and the advantages of easy availability of raw materials and low price, the use of biochar as a new type of adsorbent has been increasing in recent years[7,8]. Compared with traditional activated carbon, biochar has limited adsorption capacity for enrofloxacin in the environment. In order to enhance the adsorption capacity of biochar, the biochar is usually modified by physical and chemical methods such as acid-base and metal solution impregnation[9,10].

TiO_2 is widely used in photocatalysis research due to its good catalytic performance and non-toxic and reusable properties[11]. However, the traditional nano-TiO_2 catalytic technology has the disadvantages of easy to be inactivated and difficult to recycle, which limits its application prospects in actual production. In order to improve the catalytic efficiency of TiO_2, its often modified by ion doping[12], immobilization and other techniques.

[1]College of Resources and Environment, Jilin Agricultural University, Changchun, Jilin Province, 130118, People's Republic of China. [2]College of Plant Science, Jilin University, Changchun, Jilin Province, 130062, People's Republic of China. [3]College of Construction Engineering, Changchun Sci-Tech University, Changchun, Jilin Province, 130600, People's Republic of China. [4]These authors contributed equally: Wen Wang and Jing Zhang. *email: 491277643@qq.com; xiezl@jlu.edu.cn

Sample	Acidic group/ nmol·g^{-1}	Basic group/ nmol·g^{-1}	BET surface area/m^2·g^{-1}	Total pore volume/ cm^3·g^{-1}	Micropore volume/ cm^3·g^{-1}	Average pore width/nm
BC	0.2473	0.6399	3.5124	0.0129	0.0043	1.2940
Ti-BC	0.2437	0.6492	15.2385	0.0388	0.0130	1.1397
Ti-FBC	0.5935	0.2391	36.6511	0.2535	0.1685	0.8578
Ti-KBC	0.2012	0.9536	40.4570	0.3013	0.2243	0.6192

Table 1. Physicochemical properties of BC, Ti-BC,Ti-FBC and Ti-KBC.

Du *et al.*[13] carried out TiO_2 on carbon nanotubes by sol-gel method and founded that the degradation rate of methylene blue by TiO_2 loaded with 2% carbon nanotubes was enhanced to 90.6%. Radek Zouzelka *et al.*[14] synthesized the carbon nanotube TiO_2 porous film, and the degradation effect of the composite on 4-chlorophenol reached 96% after 0.6% carbon nanotubes supported TiO_2. Yang *et al.*[15]. Modified activated carbon fiber (ACF) with HNO_3 and synthesized a TiO_2/ACF composite, the degradation efficiency of the composite to methylene blue reached 99.99% after 30 minutes of reaction.

Previous research work has focused on the choice of carriers for immobilized TiO_2, but there have been few reports on carrier studies before loading. In this study, biochar was prepared with corn stover, and then biochar modified with iron($FeCl_3$) and alkali(KOH) were prepared by impregnationt and TiO_2/modified biochar composite was prepared by impregnation calcination method. Through the structural characterization of the composite and the photocatalytic degradation test, the degradation mechanism of enrofloxacin was clarified.

Results

Physical and chemical properties of biochar. Table 1 shows the physical and chemical properties of BC, Ti-BC, Ti-FBC and Ti-KBC. The surface acid group content of the four composites was determined by Boehm titration. The surface of BC was mainly composed of a basic group, and the basic group of Ti-BC loaded with TiO_2 was slightly increased. The content of basic groups on the surface of the prepared Ti-FBC composites decreased obviously, and the content of acidic groups increased by 2.40 times. The surface of the prepared Ti-KBC composites decreased, and the content of basic groups increased by 1.49 times. The difference in acid-base group content was one of the reasons for the difference in the ability of biochar to remove pollutants[16]. The result from BET specific surface area measurement showed that the specific surface areas of the biochar Ti-BC, Ti-FBC and Ti-KBC were 15.24, 36.65 and 40.46 m^2·g^{-1}, which increased by 4.34, 10.43 and 11.52 times compared with BC, respectively. The micropore volume of Ti-FBC and Ti-KBC accounted for 66.47% and 74.44% of the total pore volume, respectively. The surface structure and micropore content of biochar were also one of the reasons that affecting its adsorption performance[17].

Scanning electron microscopy and EDS of biochar. Figure 1 shows an SEM image of BC, Ti-BC, Ti-FBC and Ti-KBC in which the surface structure of the four carbons was evidently different. The BC has a small amount of impurity particles are attached to the surface, and the pores are occupied by a large number of debris particles. After the high temperature pyrolysis, the inner wall of the biochar collapses, and the fallen debris particles stay inside the pores, causing blockage. Compared with the SEM of BC, there were particulate matter in the carbon surface and pores of Ti-BC, Ti-FBC and Ti-KBC. Figure 2 shows EDS spectra of the four carbon. Ti-BC, Ti-FBC and Ti-KBC has Ti detected in the EDS spectra, which was not found in BC. Therefore, it was judged that the particulate matter appearing in the composite material in Fig. 1 was TiO_2. The EDS spectrum results showed that the AT(%) of Ti in Ti-BC, Ti-FBC and Ti-KBC are 0.409, 1.410, and 2.142, respectively. It can also be seen from Fig. 2 that after iron and alkali modification, the response values of Ti in the EDS spectra of Ti-FBC and Ti-KBC were stronger than that of Ti-BC, which indicating that the modified biochar can support more TiO_2 under the same loading conditions.

Infrared spectroscopy of biochar. Figure 3 shows the infrared spectrum of BC, Ti-BC, Ti-FBC and Ti-KBC. The characteristic peaks of BC, Ti-BC, Ti-FBC and Ti-KBC at 3423 cm^{-1} should be –OH stretching vibration peaks[18]. In the prepared composite material, the peak intensity here was obviously weakened, indicated that after the biochar was loaded with TiO_2, the hydroxyl group on the surface of the biochar undergoes a fracture association reaction with the TiO_2, and thus the surface hydroxyl group content was lowered. The characteristic peak at 1652 cm^{-1} was C=O bond stretching vibration. The four kinds of biochar have strong absorption peaks here, indicated that the surface of the biochar before and after loading contains carbonyl compounds such as carboxylic acid[19]. The peak at 1390 cm^{-1} was the in-plane bending vibration of $-CH_3$, which was a characteristic vibration peak of charcoal matter; the symmetric stretching vibration absorption peak of C–O–C bond at 1093 cm^{-1} [19]. The absorption band at 478–738 cm^{-1} in Fig. 2 was due to the stretching vibration of the Ti–O–Ti bond and the Ti-O bond in the TiO_2 molecule[13]. This characteristic peak appears only in the infrared spectrum of Ti-BC, Ti-FBC and Ti-KBC and is not found in BC, which indicated that TiO_2 has been supported on the surface of the modified biochar.

XRD of biochar. Figure 4 shows the XRD patterns of BC, Ti-BC, Ti-FBC and Ti-KBC. The four biochar have obvious diffraction peaks at $2\theta = 26.6°$, and the graphite microcrystal diffraction peak d_{002}[20] was determined according to the analysis result of Jade. After the corn stalk biochar was modified and loaded, the diffraction peak intensity was weakened at $2\theta = 26.6°$, and the crystallinity decreased. The surface defects and porosity of the biochar increased, so the specific surface area of the composite material also increased. From the XRD patterns

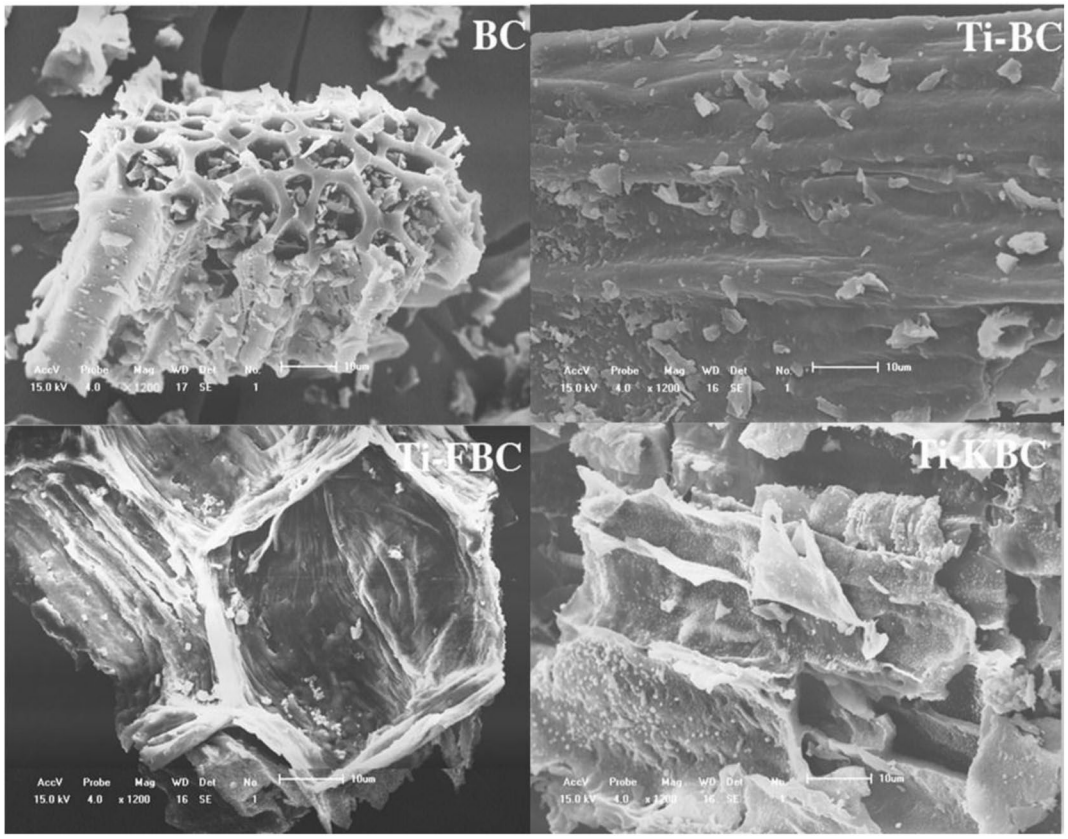

Figure 1. Scanning electron micrograph of BC, Ti-BC, Ti-FBC and Ti-KBC (1200 times).

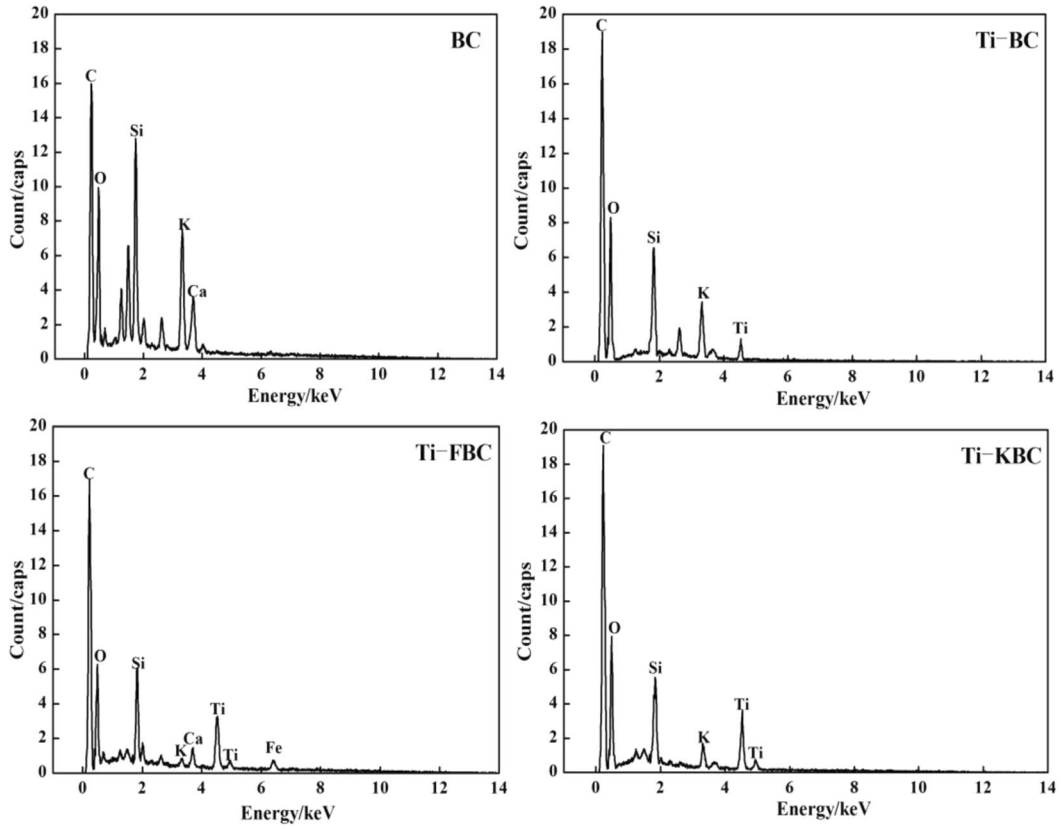

Figure 2. Energy spectra of BC, Ti-BC, Ti-FBC and Ti-KBC.

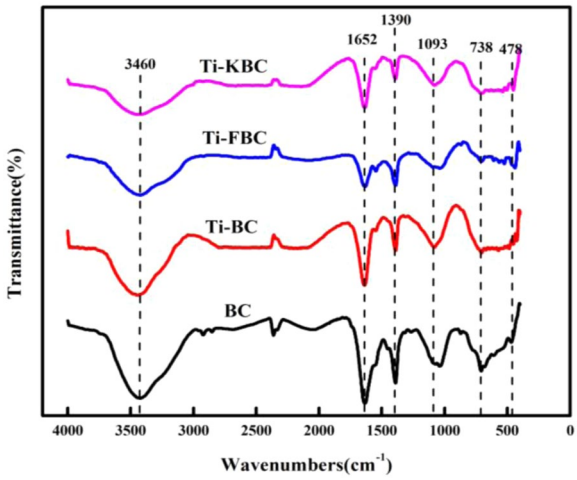

Figure 3. Infrared spectra of BC, Ti-BC, Ti-FBC and Ti-KBC.

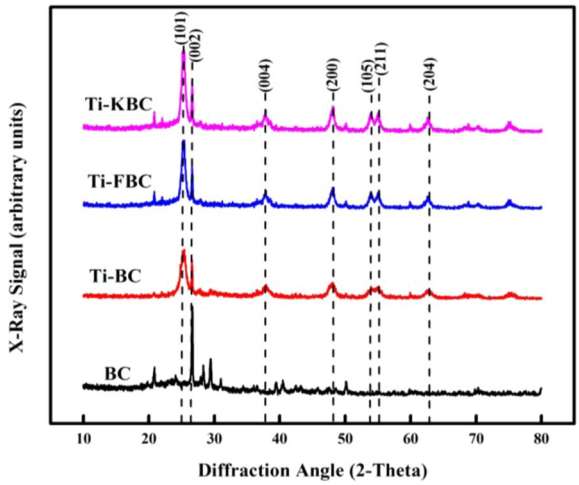

Figure 4. X-ray diffraction patterns of BC, Ti-BC, Ti-FBC and Ti-KBC.

of Ti-BC, Ti-FBC and Ti-KBC in Fig. 4, the diffraction peaks located at 25.26°, 37.88°, 48.08°, 53.94°, 55.00° and 62.56° were corresponded to (101), (004), (200), (105), (211) and (204) crystal planes of anatase TiO_2 (ICSD: 01–089). The results revealed that TiO_2 supported on each biochar material existed in an anatase state under high temperature calcination, this was consistent with the analysis results of the EDS spectra.

XPS of biochar. Figure 5 shows the XPS spectra of BC, Ti-BC, Ti-FBC and Ti-KBC. From Fig. 5, it can be seen that the C1s and O1s lines appear in the XPS spectra of the four biochar. Compared with BC, Ti2p lines appear in the spectra of Ti-BC, Ti-FBC and Ti-KBC, confirming the presence of Ti element in the composite, which was consistent with the previous characterization results of EDS, XRD, etc. In order to determine the existence form of Ti element, the lines near the Ti2p peak in Ti-BC, Ti-FBC and Ti-KBC are enlarged to obtain the fine spectrum of Ti2p, as shown in Fig. 6. It can be seen from Fig. 6 that the Ti2p energy levels of Ti-BC, Ti-FBC and Ti-KBC are split into two energy levels due to the spin-orbit coupling of the electrons. Peak fitting was performed based on the contribution of different titanium oxides to Ti2p. The peaks at 458.5, 458.9, and 458.8 eV corresponded to the peaks of Ti2p3/2, and the peaks at 464.4, 464.7, and 464.8 eV corresponded to Ti2p1/2 peaks. The actual measurement results are close to the theoretical values Ti2p3/2 (458.8 eV) and Ti2p1/2 (462.2 eV), indicated that the Ti valence state in Ti-BC, Ti-FBC and Ti-KBC is Ti^{4+} and exists as TiO_2[21].

UV-vis DRS of biochar. Figure 7(a,b) are the UV-vis DRS spectra and band gap of Ti-BC, Ti-FBC and Ti-KBC. It can be seen from Fig. 7(a) that the composite material after TiO_2 loading has strong absorption in the ultraviolet region. Compared with Ti-BC, the maximum light absorption edges of Ti-FBC and Ti-KBC are red-shifted and show higher light absorption in the visible light region. In order to further explore the optical properties of biochar, the band gap E_g of Ti-BC, Ti-FBC and Ti-KBC was calculated by Tauc plot Eq. (1)[22]. As shown in Fig. 7(b), according to the Eq. (1), the forbidden band widths of Ti-BC, Ti-FBC and Ti-KBC were calculated to be 2.69 eV, 2.52 eV, and 2.41 eV, respectively.

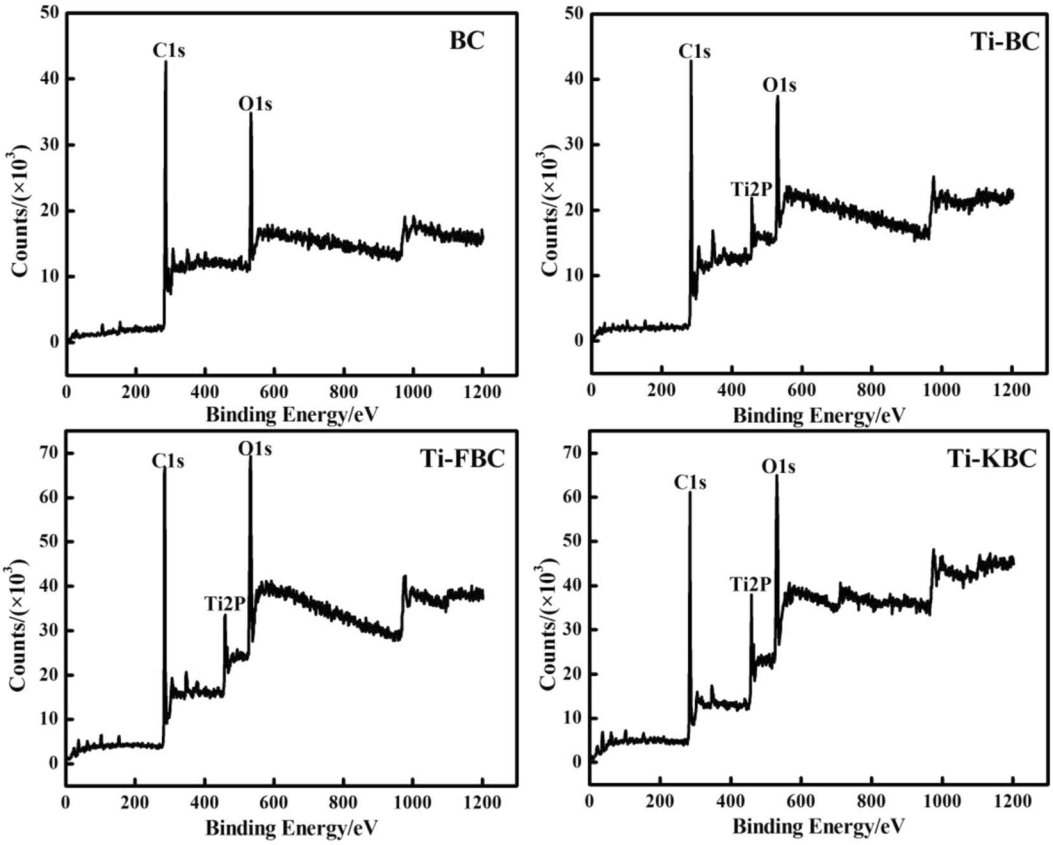

Figure 5. XPS spectra of BC, Ti-BC, Ti-FBC and Ti-KBC.

$$(\alpha h\nu)^{1/n} = A\left(h_\nu - E_g\right) \tag{1}$$

Where α is the absorption coefficient, and Abs value is used in this article; h is the Planck constant, 6.626×10^{-34} J·s; ν is the frequency, $h\nu = hc/\lambda$, c is the speed of light, 3×10^8 m·s^{-1}, λ is the wavelength of light, m; TiO_2 is an indirect bandgap semiconductor, $n = 2$; A is a constant; Eg is the band gap, eV. Plot $h\nu$ as the abscissa $(\alpha hv)^{1/2}$ as the ordinate, and then tangent to get Eg.

Photodegradation kinetics test. Figure 8(a) shows the curve of the equilibrium concentration of enrofloxacin over time in the BC, Ti-BC, Ti-FBC and Ti-KBC systems under UV light. According to the Fig. 8(a), after the solution system has undergone dark reaction absorption-desorption equilibrium, the equilibrium concentrations of enrofloxacin in the BC, Ti-BC, Ti-FBC, and Ti-KBC systems were 50.00, 50.76, 54.80, and 55.45 mg·L^{-1}, respectively. Under 15 W UV lamp (254 nm) irradiation, the equilibrium concentration of enrofloxacin in the solution gradually decreases with the increase of the photochemical reaction time, and the equilibrium concentration of enrofloxacin tended to equilibrium after 60 minutes of the photocatalytic time. After two stages of adsorption-photolysis, the equilibrium concentrations of enrofloxacin in the BC, Ti-BC, Ti-FBC, and Ti-KBC degradation systems were 46.97, 39.43, 29.78, and 15.50 mg·L^{-1}, and the degradation rates of enrofloxacin were 53.01%, 60.60%, 70.32%, and 84.65%, respectively, according to Eq. (1).

The kinetic analysis of enrofloxacin photodegradation was calculated according to Eqs. (3), (4). Figure 8(b) was a photocatalytic first-order kinetics fit curve of enrofloxacin on BC, Ti-BC, Ti-FBC and Ti-KBC for 60 min, and Table 2 showed the rate parameters of photocatalytic degradation of enrofloxacin by different biochar and the proportion of adsorption under dark reaction. As can be seen from Table 2, the degradation rates of enrofloxacin by BC, Ti-BC, Ti-FBC and Ti-KBC were 0.0008, 0.0038, 0.0090, and 0.0101 min^{-1}, respectively. After loaded TiO_2, the degradation rates of enrofloxacin by Ti-BC, Ti-FBC and Ti-KBC were increased by 4.75, 11.25, 25.13 times, respectively. The degradation rate of enrofloxacin was significantly improved by the Ti-FBC and Ti-KBC.

$$\eta = \frac{C_0 - C_t}{C_0} \times 100\% \tag{2}$$

$$\frac{dC_t}{dt} = -rC_0 + b \tag{3}$$

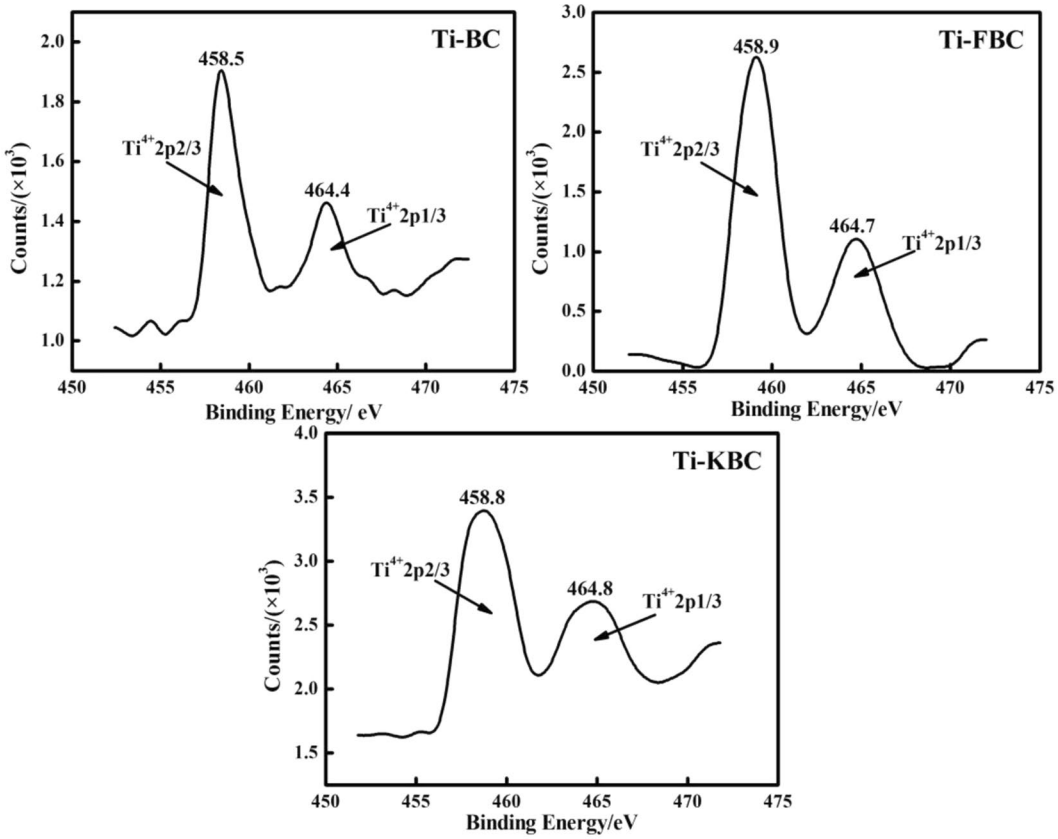

Figure 6. Ti2p peaks of Ti-BC, Ti-FBC and Ti-KBC.

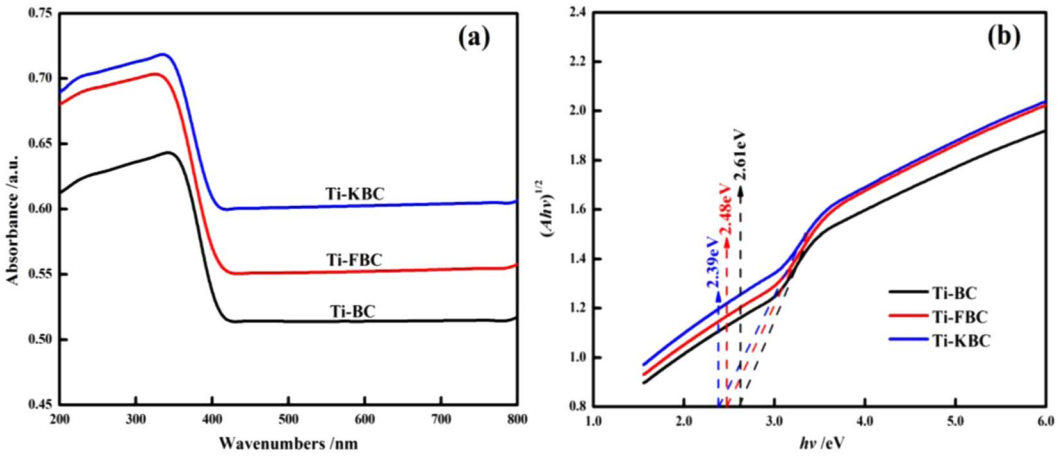

Figure 7. The UV-vis DRS adsorption spectra (**a**) and the band gap (**b**) of Ti-BC, Ti-FBC and Ti-KBC.

Where C_0, and C_t are the concentrations of enrofloxacin in the solution at the initial, and time t, mg·L^{-1}; η is the degradation rate of enrofloxacin, %; t is the reaction time, min; r is the first-order power Learning constant, min^{-1}; b is a constant.

According to Eq. (3), the integral is:

$$\ln\frac{C_t}{C_0} = -rt + b \tag{4}$$

Degradation effect of enrofloxacin at different initial concentrations. Figure 9 shows the degradation of enrofloxacin by BC, Ti-BC, Ti-FBC and Ti-KBC at different initial concentrations. When the dosages of BC, Ti-BC, Ti-FBC and Ti-KBC were all 2.5 g·L^{-1}, within the test concentration range, the degradation

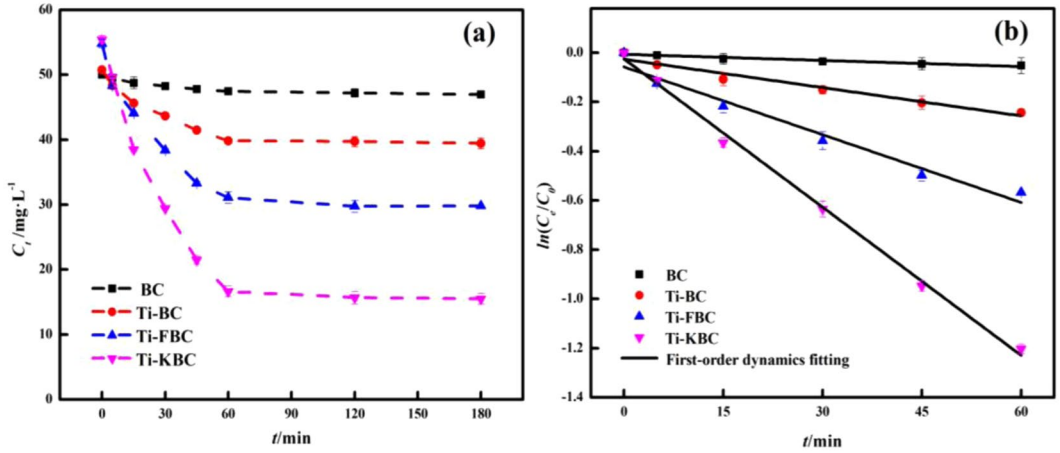

Figure 8. Photocatalytic kinetic curves(**a**) and fitting curves(**b**) of enrofloxacin by BC, Ti-BC, Ti-FBC and Ti-KBC.

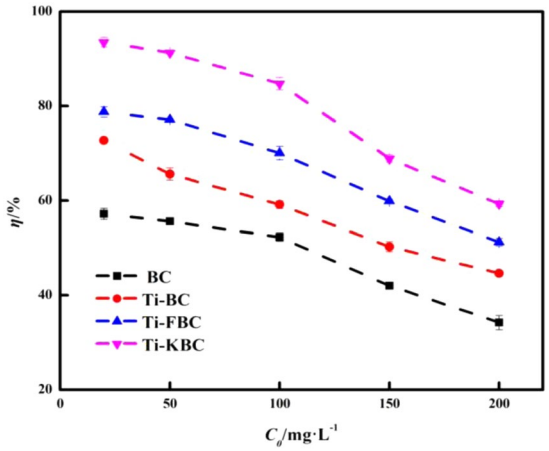

Figure 9. Effects of different initial concentrations on the degradation rate of enrofloxacin.

Sample	Kinetic equations	r (min^{-1})	R^2
BC	$ln(C_e/C_0) = -0.0008t + 0.0065$	0.0008	0.9415
Ti-BC	$ln(C_e/C_0) = -0.0038t + 0.0260$	0.0038	0.9643
Ti-FBC	$ln(C_e/C_0) = -0.0092t + 0.0057$	0.0092	0.9692
Ti-KBC	$ln(C_e/C_0) = -0.0201t + 0.0245$	0.0201	0.9970

Table 2. Rate parameters for catalytic degradation of enrofloxacin by BC, Ti-BC, Ti-FBC and Ti-KBC.

rates of four biochar on enrofloxacin decreased with the increase of the initial concentration. Under different initial concentration conditions, the degradation rates of the four biochar for enrofloxacin were order by Ti-KBC > Ti-FBC > Ti-BC > BC.

Degradation effect of enrofloxacin at different initial pH values. Figure 10 shows the changes of BC, Ti-BC, Ti-FBC and Ti-KBC degradation efficiency of enrofloxacin under different initial pH conditions. It can be seen from Fig. 11 that with the increase of the initial pH value of the solution, the degradation rates of the four biochar on enrofloxacin all increase first and then decrease. In different pH values, the degradation rates of the four biochar for enrofloxacin were order by Ti-KBC > Ti-FBC > Ti-BC > BC. When the initial pH = 5.0, BC, Ti-BC, Ti-FBC and Ti-KBC showed the optimum degradation efficiency of enrofloxacin, with the maximum degradation rates of 53.60%, 61.48%, 71.49% and 85.25%, respectively.

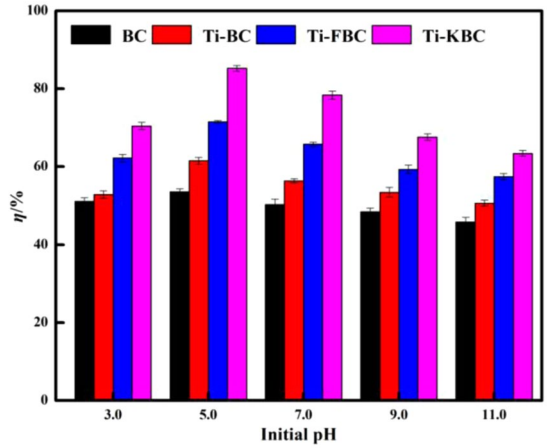

Figure 10. Effect of different initial pH values on the degradation rate of enrofloxacin.

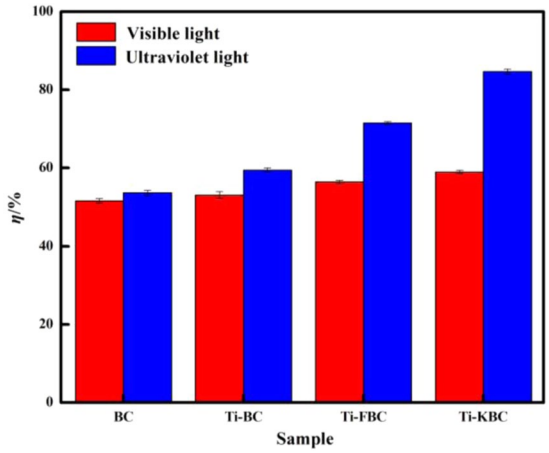

Figure 11. Effects of different light conditions on the degradation rate of enrofloxacin.

Degradation effect of enrofloxacin by different light sources. Figure 11 shows the degradation effect of BC, Ti-BC, Ti-FBC and Ti-KBC on enrofloxacin under different illumination conditions. After dark reaction adsorption-desorption equilibrium and 60 min of visible light irradiation, the degradation rates of enrofloxacin by BC, Ti-BC, Ti-FBC and Ti-KBC under the irradiation of visible light were 51.58% and 53.11%, 56.41%, 58.97%, respectively. After UV light irradiation for 60 min, the degradation of enrofloxacin by each biochar was 53.60%, 59.48%, 71.49%, and 84.65%, respectively. In summary, the degradation of enrofloxacin by BC, Ti-BC, Ti-FBC and Ti-KBC was better under ultraviolet light irradiation than that under visible light irradiation.

Identification of photodegradable active substances. The main active substances of enrofloxacin catalyzed by the supported materials were investigated by the quenching test. Figure 12 shows the kinetic fit curve of the enzymatic degradation of enrofloxacin by adding different quenchers. The specific parameters are shown in Table 3. The active material contribution rate was calculated according to Eq. (5). Table 3 shows that the degradation rate of enrofloxacin was 0.0201 min^{-1} in the unquenched group. After Benzoquinone was added, $O_2\bullet^-$ did not participate in catalytic degradation reaction in the solution. At this time, the degradation rate of enoxacin decreased to 0.0065 min^{-1}. According to Eq. (5), the contribution rate of $O_2\bullet^-$ was about 67.66%. In the experimental group with Isopropanol, the degradation rate was 0.0175 min^{-1}, and •OH did not participate in the reaction. It was calculated that •OH contributed about 12.94% to catalytic degradation. After adding KI to the solution, the •OH and h^+ (holes) in the reaction system did not participate in the degradation process. The degradation rate of the test group was 0.0139 min^{-1}, and the degradation contribution rate was about 30.85%. By compared and analyzed the contribution rate of different active substances to enrofloxacin degradation, it can be concluded that the main active substance in this reaction system was $O_2\bullet^-$.

$$R \approx \frac{r - r_e}{r} \times 100\% \tag{5}$$

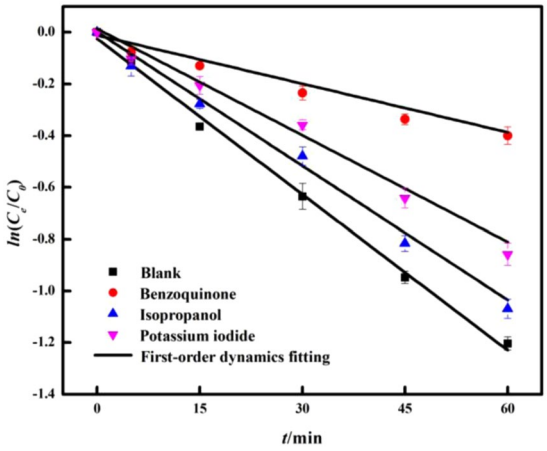

Figure 12. Kinetic fit curve of catalytic degradation of enrofloxacin by different quenchers.

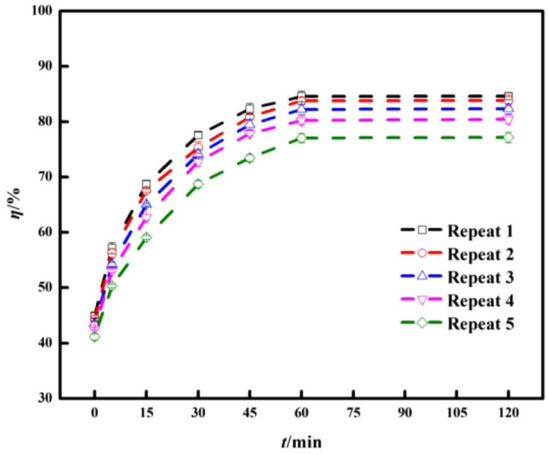

Figure 13. Effect of different cycle times on the degradation efficiency of enrofloxacin.

Quencher	Kinetic equations	r (min^{-1})	R^2
Blank	$ln(C_e/C_0) = -0.0201t - 0.0245$	0.0201	0.9415
Benzoquinone	$ln(C_e/C_0) = -0.0065t - 0.0279$	0.0065	0.9643
Isopropanol	$ln(C_e/C_0) = -0.0175t - 0.0105$	0.0175	0.9692
Potassium iodide	$ln(C_e/C_0) = -0.0139t + 0.0029$	0.0139	0.9900

Table 3. Catalytic degradation rate parameters of enrofloxacin by different quenchers.

Where R is the contribution rate of different active substances to the degradation of enrofloxacin, %; r is the first-order kinetic rate constant of enrofloxacin photodegradation measured by the unquenched test group, min^{-1}; r_0 is different The first order kinetic rate parameter measured after the quencher, min^{-1}.

Analysis of cyclic test of TiO_2-modified biochar. The photocatalytic test showed that Ti-KBC had the highest degradation rate of enrofloxacin. Therefore, the cycle test was performed with Ti-KBC, and the results were shown in Fig. 13. At the initial concentration of enrofloxacin 100 mg·L^{-1} and the dosages of Ti-KBC 2.5 g·L^{-1}, as the number of cycles increased, the degradation rate of enrofloxacin gradually decreased from 84.63% to 77.14%, which was still higher than that of BC, Ti-BC and Ti-FBC.

Discussion

In order to study the degradation mechanism of enrofloxacin by BC, Ti-BC, Ti-FBC and Ti-KBC, we used EDS, XRD, FT-IR, XPS, etc. to characterize the structure of four kinds of biochar. After modification, the surface of the biochar can adhere to more TiO_2, so the Ti-FBC and Ti-KBC have a larger specific surface area, and t he stronger the degradation performance of pollutants for the modified biochar. That the loaded TiO_2 was

uniformly distributed on the surface and the pores of the composite(biochar) not only provided the sufficient sites for adsorbing enrofloxacin, but also had a good photocatalytic activity for the degradation of enrofloxacin. By compared the unmodified biochar, after the iron modification and alkalization modification, the more TiO_2 can be supported on the surface of the biochar, so the degradation of enrofloxacin were better.

In the photocatalytic degradation reaction, the smaller the band gap of the material, the easier it is to be excited by visible light. The more photo-generated electrons in the valence band transition to the conduction band, the more holes in the valence band participate in the oxidation reaction, and the degradation efficiency higher[23]. The UV-vis DRS analysis shows that Ti-KBC has the lowest band gap, so the slower the recombination rate of photogenerated electron-hole pairs, and the photocatalytic activity of the Ti-KBC was improved, which was consistent with the results measured by the photodegradation test.

TiO_2 supported on the surface of Ti-BC, Ti-FBC and Ti-KBC generated the electron-hole pair and reacted in the solution system to generate strong oxidizing active groups such as hydroxyl radical (•OH) and superoxide ion radical ($O_2\bullet^-$)[24] under the excitation of ultraviolet light, therefore, the degradation rate of enrofloxacin by TiO_2-loaded biochar improved effectively. Compared with unmodified biochar, the modified biochar had more abundant specific surface area and pore structure, and could attach more TiO_2, consequently, the lifetime of photogenerated electrons increased and the photodegradation efficiency improved significantly. In addition, the basic oxygen-containing groups on the surface of the alkalized modified biochar increased greatly, and these oxygen-containing groups acted on the nano-TiO_2 particles[25], which made Ti-KBC had the most efficient degradation of enrofloxacin.

Enrofloxacin, being an ionic organic compound with a dissociation constant of $pK_{a1} = 6.02$ and $pK_{a2} = 8.25$[26], exists in different ionic forms at different pH. Since the surface of Ti-BC, Ti-FBC and Ti-KBC were negatively charged, this favors enrofloxacin adsorption in the cationic form. When the $pH < 5.0$, the adsorption of enrofloxacin on the biochar reduced obviously because a large amount of H^+ in the solution competed with the cation form of enrofloxacin. At the pH range of 5.0–6.02, it was the pH environment in which biochar had the best adsorption effect on enrofloxacin, and further the composite material had the best degradation effect on enrofloxacin. At $pH > 6.02$, enrofloxacin was mainly anionic in solution, which was not conducive to adsorption by negatively charged BC, Ti-BC, Ti-FBC, and Ti-KBC on the surface, leading to a decrease in the amount of adsorption, which limited the enrofloxacin degradation. When the biochar was added in a certain amount, the active substances produced in the solution system were limited. As the initial concentration of enrofloxacin in the solution increased, the produced active substances could not degrade enough enrofloxacin, thus leading to the degradation rate of enrofloxacin gradually decreased.

Due to the photocatalytic effect of TiO_2, enrofloxacin adsorbed on Ti-KBC was degraded into small molecules under the irradiation of ultraviolet light, the re-adsorption capacity of Ti-KBC was enhanced, and the reuse of Ti-KBC performance was also improved. It was resulted in the higher the degradation rate of Ti-KBC for enrofloxacin through five cycles of tests.

Conclusions

In the study, the TiO_2-modified biochar was synthesized by impregnation and calcination. The SEM, EDS, FT-IR, XRD, XPS analysis showed that TiO_2 was loaded on the composite material in anatase state. Through UV-vis DRS analysis of biochar, the band gaps of Ti-FBC and Ti-KBC were lower and have higher photocatalytic activity. Under 15 W UV lamp (254 nm) irradiation, the photodegradation reaction of the unmodified biochar(BC), TiO_2-biochar(Ti-BC), TiO_2-ironized biochar(Ti-FBC) and TiO_2-alkaline biochar(Ti-KBC) for enrofloxacin conformed to the first-order kinetic model. After 60 minutes of UV irradiation, the maximum degradation effect was achieved and the Ti-KBC showed the optimum degradation effect of enrofloxacin. At the solution pH 5.0 and the dosage of Ti-KBC 2.5 $g \cdot L^{-1}$, the degradation rate of 100 $mg \cdot L^{-1}$ enrofloxacin reached 85.25%. After five cycles of tests, the degradation rate of Ti-KBC for enrofloxacin solution reached 77.14%, which indicated that the Ti-KBC was more feasible to degrade enrofloxacin.

Materials and Methods

The test primary biochar was made from corn stalk through a 20 mesh sieve, pyrolyzed in a muffle furnace at 773 K for 3 h, and after pyrolysis, cooled to room temperature, and passed through a 60 mesh sieve. The sample was marked as BC.

Synthesis of TiO_2-biochar composite. First, takeing 25 ml of absolute ethanol into a beaker, and adding 2 ml of butyl titanate slowly under stirring with a magnetic stirrer, thorough mixing, and then adding 1 ml of distilled water, glacial acetic acid and nitric acid,repectively, through mixing again, and continue to add 1 ml of distilled water, glacial acetic acid and nitric acid, repectively, stirring for 30 min and finally adding 5 g of biochar, contnue to stir for 30 min, the mixture obtained was dried in an oven at 378 K, andthen, calcined at 773 K for 3 h in a muffle furnace, and finally cooled to room temperature to obtain a composite material (marked as Ti-BC). Secondly, BC(10.0 g) was added to 100 mL of 0.1 $mol \cdot L^{-1}$ Fe^{3+} solution which was fully soaked at a ratio of 1:10, and placedon a constant temperature agitator, oscillated every 8 h and aged for 24 h. After the reaction was completed, it is washed repeatedly with distilled water until neutral, placed in an oven (378 K) for 24 h. After modification, the operations of loading TiO_2 were the same as Ti-BC, the sample was marked as Ti-FBC. Thirdly, BC(10.0 g) was added to 100 ml of 25% KOH solution and fully soaked at a 1:10 impregnation ratio. Other operations were the same as Ti-FBC, the sample was marked as Ti-KBC.

Photocatalytic performance test. Weigh 0.5000 g of BC, Ti-BC, Ti-FBC and Ti-KBC into a 250 ml beaker and add 200 ml of enrofloxacin solution with an initial concentration of 100 $mg \cdot L^{-1}$. At 298 K, the temperature was kept away from light for 12 h. After reached the adsorption-desorption equilibrium, the photodegradation

test was performed under the irradiation of ultraviolet light (254 nm) generated by a 15 W ultraviolet lamp. When the degradation times were 0, 15, 30, 45, 60, 120, 180, 240, 300, 360 min, sample the solution separately. The supernatant was passed through a 0.45 μm membrane, and the content of enrofloxacin in the solution was determined by a liquid chromatograph. The initial enrofloxacin concentration was varied to 20, 50, 100, 150, 200 $mg{\cdot}L^{-1}$, to explore the effects of different initial concentrations on photodegradation. Adjust the initial pH of the solution to 3.0, 5.0, 7.0, 9.0, 11.0, to explore the effects of different initial pH on photodegradation. Changing the light source of photodegradation and to explore the degradation characteristics in both UV(15 W) and visible light(15 W) conditions. All the above experiments were performed with 3 groups of duplicates, and the data were fitted and analyzed using origin 8.5.

Active substance detection. Weigh four 0.5000 g Ti-KBC into a 250 ml beaker and add 200 ml of enrofloxacin solution with an initial concentration of 100 $mg{\cdot}L^{-1}$. One directly subjected to photocatalytic degradation test, the other three were added with p-benzoquinone ($O_2{\bullet}^-$ quencher[27], isopropanol (•OH quencher[28], potassium iodide (•OH and h^+ quencher[29]. After the dark reaction is over, the photocatalytic test is started. The above tests were all set to 3 groups of repetitions.

Cycle test of TiO_2-modified biochar. Ti-KBC was used as the sample to perform the cycle test. Weigh 0.5000 g of Ti-KBC into a 250 ml beaker and add 200 ml of enrofloxacin solution with an initial concentration of 100 $mg{\cdot}L^{-1}$, initial pH = 5.0. After the adsorption-degradation reaction ended, filter out the remaining liquid and add 100 $mg{\cdot}L^{-1}$ again of enrofloxacin solution and continue the reaction. Setting up 5 times cycle tests according the above test step.

Characterization of biochar. The surface acidic and basic group content of biochar is determined according to the Boehm method[30]; Specific surface area and pore structure of biochar was determined by specific surface area and pore size analyzer[31]; Microscopic characterization and EDS analysis of biochar using scanning electron microscope (SSX-550)[32]; The distribution of functional groups on the surface of biochar was analyzed by infrared spectrometer(FTIR)[33]; The crystal structure of biochar was determined by X-ray diffraction spectroscopy (XRD) and X-ray photoelectron spectroscopy (XPS)[33]; The optical properties of the composites were measured by a UV-visible spectrum scanner(UV-vis DRS).

Determination of enrofloxacin. Chromatographic conditions: column (ZORBAX Eclipse XDB-C18 150 mm × 4.6 mm); Column temperature 303 K; injection volume 20 μL; Determination of enrofloxacin mobile phase was methanol: water = 30:70 (V/V) The flow rate was 1.0 $mL{\cdot}L^{-1}$, the UV detection wavelength was 275 nm, and the retention time was 4.6 min.

Received: 23 November 2019; Accepted: 16 March 2020;
Published online: 20 April 2020

References

1. Roth, N. *et al*. Effect of an organic acids based feed additive and enrofloxacin on the prevalence of antibiotic-resistant E. coli in cecum of broilers. *Poultry Science*, **96**, 4053–4060, https://doi.org/10.3382/ps/pex232 (2017).
2. Yang, D. Y. *et al*. Analysis of monitoring results of veterinary drug residues in poultry foods in Shenzhen in 2017. *Journal of Food Safety & Quality Testing* **9**, 6338–6342, https://doi.org/10.3969/j.issn.2095-0381.2018.23.045 (2018).
3. Janusch, F. *et al*. Determination of fluoroquinolones in chicken feces - a new liquid-liquid extraction method combined with LC-MS/MS. *Environmental Toxicology & Pharmacology* **38**, 792–799, https://doi.org/10.1016/j.etap.2014.09.011 (2014).
4. Gao J. H. Adsorption and photolysis behavior of antibiotic sulfathiazole and enrofloxacin in water environment. *Lanzhou University* (2016).
5. Idris Y. R. *et al*. Kinetic Modelling of the Pyrolysis of Biomass for the Development of Charcoal Briquette. *IOP Conference Series Materials Science and Engineering* **206**, https://doi.org/10.1088/1757-899x/206/1/012063 (2017).
6. Parshetti, G. K., Chowdhury, S. & Balasubramanian, R. Biomass derived low-cost microporous adsorbents for efficient CO2 capture. *Fuel* **148**, 246–254, https://doi.org/10.1016/j.fuel.2015.01.032 (2015).
7. Tong, M. X. *et al*. Determination of PAHs in Water Using Bamboo Charcoal as a Solid-phase Extraction Adsorbent By Constant-wavelength Synchronous Fluorescence Spectrometry. *Fujian Analysis & Testing* **518–523**, 1501–1505, https://doi.org/10.4028/www.scientific.net/AMR.518-523.1501 (2017).
8. Zhang, S. *et al*. Porous magnetic carbon sheets from biomass as an adsorbent for the fast removal of organic pollutants from aqueous solution. *Journal of Materials Chemistry A* **2**, 4391–4397, https://doi.org/10.1039/C3TA14604A (2014).
9. Kołodyńska, D. *et al*. Investigations of Heavy Metal Ion Sorption Using Nanocomposites of Iron-Modified Biochar. *Nanoscale Research Letters* **12**, 433, https://doi.org/10.1186/s11671-017-2201-y (2017).
10. Wan, S., Hua, Z., Sun, L., Bai, X. & Liang, L. Biosorption of nitroimidazole antibiotics onto chemically modified porous biochar prepared by experimental design: Kinetics, thermodynamics, and equilibrium analysis. *Process Safety and Environmental Protection* **104**, 422–435, https://doi.org/10.1016/j.psep.2016.10.001 (2016).
11. Yuan, Q. *et al*. Surface Chemistry of Formaldehyde on Rutile TiO\r2\r, (110) Surface: Photocatalysis vs Thermal-Catalysis. *The Journal of Physical Chemistry C* **118**, 20420–20428, https://doi.org/10.1021/jp5061733 (2014).
12. Chen, Y. *et al*. Preparation And Photocatalytic Performance Of F-TiO_2 Photocatalyst. *IOP Conference Series Earth and Environmental Science* **189**, 032005, https://doi.org/10.1088/1755-1315/189/3/032005 (2018).
13. Du, R. A. *et al*. Synthesis of multi-walled carbon nanotubes/TiO_2 composites and their photocatalytic properties. *Nonferrous Metals Science and Engineering* **10**, 75–84, https://doi.org/10.13264/j.cnki.ysjskx.2019.05.012 (2019).
14. Zouzelka, R. *et al*. Photocatalytic activity of porous multiwalled carbon nanotube-TiO_2 composite layers for pollutant degradation. *Journal of Hazardous Materials* **317**, 52–59, https://doi.org/10.1016/j.jhazmat.2016.05.056 (2016).
15. Yang, Y. *et al*. Photocatalytic degradation of methylene blue in water by nitric acid-modified activated carbon fiber-supported TiO_2. Advanced Chemical. *Materials* **44**, 105–107 (2016).
16. Zhu, Y. T. *et al*. Adsorption characteristics of biochar prepared by corn stalk alkalization on zinc. *Journal of Agro-Environment Science* **37**, 179–185 (2018).

17. Wang, W. *et al*. Adsorption of enrofloxacin on acid/alkali-modified corn stalk biochar. *Spectroscopy Letters* **52**, 367–375, https://doi.org/10.1080/00387010.2019.1648296 (2019).
18. Kan, Z. *et al*. A New Benzoxazine Containing Benzoxazole-Functionalized Polyhedral Oligomeric Silsesquioxane and the Corresponding Polybenzoxazine Nanocomposites. *Macromolecules* **46**, 2696–2704, https://doi.org/10.1021/ma400243t (2013).
19. Moraillon, A. *et al*. Amidation of Monolayers on Silicon in Physiological Buffers: A Quantitative IR Study. *Journal of Physical Chemistry C* **112**, 7158–7167, https://doi.org/10.1021/jp7119922 (2008).
20. Barnakov, C. N. *et al*. X-ray diffraction analysis of the crystal structures of different graphites. *Solid Fuel Chemistry* **49**, 25–29, https://doi.org/10.3103/S0361521915010036 (2015).
21. Li, J. *et al*. Contact potential barriers and characterization of Ag-doped composite TiO_2 nanotubes. *Journal of Physics and Chemistry of Solids* **75**, 505–511, https://doi.org/10.1016/j.jpcs.2013.12.011 (2014).
22. Estrada, R. *et al*. The optical band gap of LiTaO3 and Nb2O5 -doped LiTaO3 thin films based on Tauc Plot method to be applied on satellite. *IOP Conference Series Earth and Environmental Science* **54**, 012092, https://doi.org/10.1088/1755-1315/54/1/012092 (2017).
23. Hao, D. Z. *et al*. Structure, optical and photocatalytic properties of TiO_2 films modified by silver nanoparticles. *Optoelectronics. Laser* **4**, 376–381 (2019).
24. Borji, S. H. *et al*. Investigation of photocatalytic degradation of phenol by Fe(III)-doped TiO_2 and TiO_2 nanoparticles. *Journal of Environmental Health Science & Engineering* **12**, 101, https://doi.org/10.1186/2052-336X-12-101 (2014).
25. Chen, J., Chen, Q. & Ma, Q. Influence of surface functionalization via chemical oxidation on the properties of carbon nanotubes. *Journal of Colloid & Interface Science* **370**, 32–38, https://doi.org/10.1016/j.jcis.2011.12.073 (2012).
26. Cárdenas, Y., Gina, M., Beltrán & José, L. Dissociation constants and octanol–water partition equilibria for several fluoroquinolones. *Journal of Chemical & Engineering Data* **60**, 3327–3332, https://doi.org/10.1021/acs.jced.5b00556 (2015).
27. Peng, T. *et al*. Plasmon-induced reduction of bromate with Au–Ag–AgI/Al2O3 under visible-light irradiation. *Journal of Chemical Technology & Biotechnology* **89**, 1425–1431, https://doi.org/10.1002/jctb.4227 (2014).
28. Song, W. *et al*. Free Radical Destruction of β-Blockers in Aqueous Solution. *Environmental Science & Technology* **42**, 1256–1261, https://doi.org/10.1021/es702245n (2008).
29. Wang, S. *et al*. Synthesis and characterization of g-C3N4/Ag3VO4 composites with significantly enhanced visible-light photocatalytic activity for triphenylmethane dye degradation. *Applied Catalysis B Environmental* **144**, 885–892, https://doi.org/10.1016/j.apcatb.2013.08.008 (2014).
30. Tsechansky, L. & Graber, E. R. Methodological limitations to determining acidic groups at biochar surfaces via the Boehm titration. *Carbon* **66**, 730–733, https://doi.org/10.1016/j.carbon.2013.09.044 (2014).
31. Sigmund G. *et al*. Biochar total surface area and total pore volume determined by N2 and CO2 physisorption are strongly influenced by degassing temperature. *Science of The Total Environment* **580**, 770–775, https://doi.org/10.1016/j.scitotenv.2016.12.023 (2017).
32. Qi, X. *et al*. Water-assisted and controllable synthesis of core/shell/shell structured carbon-based nanohybrids, and their magnetic and microwave absorption properties. *Scientific Reports* **7**, 9851, https://doi.org/10.1038/s41598-017-10352-8 (2017).
33. Chen L. Microstructure characterization and performance analysis of carbon fiber. *Southwest University of Science and Technology*. (2015)

Acknowledgements

The article was funded by the National Natural Science Foundation(31672051),the Major science and technology projects in Jilin Province (2018020101018SF), and the National Key Research and Jilin Province Natural Science Foundation (20180101086JC) for assistance in this research.

Author contributions

W.W. and J.Z. are the joint first author, they designed and conducted the preparation of materials and photodegradation tests and wrote the main manuscript text and fgures. T.Y.C. and J.S. assisted in performance of photodegradation experiments and manuscript writing. X.L.M., Y. J.W. and J.H.W. provided project design, oversight, and manuscript additions including. Z.L.X. completed the correction and format check of the manuscript.

Competing interests

The authors declare no competing interests.

Additional information

Correspondence and requests for materials should be addressed to X.M. or Z.X.

Reprints and permissions information is available at www.nature.com/reprints.

Publisher's note Springer Nature remains neutral with regard to jurisdictional claims in published maps and institutional affiliations.